Manuscript

Click here to view linked References

Hydrogen absorption and desorption properties of Mn-based Mn–Al alloy investigated using synchrotron radiation x-ray diffraction technique

Reina Utsumi [a,*], Saya Ajito [b, 1], Shigeyuki Takagi [a], Yuki Nakahira [c], Hiroyuki Saitoh [a], Tetsu Watanuki [a], Toyoto Sato[b], Eiji Akiyama [b], Shin-ichi Orimo [b,d]

[a] National Institutes for Quantum Science and Technology (QST), 1-1-1, Kouto, Sayo-cho, Sayo-gun, Hyogo 679-5148, Japan

[b] Institute for Materials Research, Tohoku University, 2-1-1, Katahira, Aoba-ku, Sendai, Miyagi 980-8577, Japan

[c] Graduate School of Advanced Science and Engineering, Hiroshima University, 1-7-1, Kagamiyama, Higashihiroshima, Hiroshima 739-8521, Japan

[d] Advanced Institute for Materials Research (WPI-AIMR), Tohoku University, 2-1-1, Katahira, Aoba-ku, Sendai, Miyagi 980-8577, Japan

*corresponding author: utsumi.reina@qst.go.jp

[1] (Present address) National Institute for Materials Science (NIMS), 1-2-1, Sengen, Tsukuba, Ibaraki 305-0047, Japan

Keywords: Metal hydride, High-pressure synthesis, Synchrotron radiation x-ray diffraction, Mn–Al alloy

Abstract

One of the key challenges associated with hydrogen storage alloys is reducing material costs. The conventional design guideline for hydrogen storage alloys, consisting of metals with high and low affinities for hydrogen, limits the choice of elements, so that the discovery of novel low-cost alloy hydrides is all the more challenging. To address this challenge, we attempted to hydrogenate alloys consisting of only metal with a low affinity for hydrogen, especially cost-effective transition metal and aluminum. In this study, Mn-based Mn–Al hydrides were synthesized. The crystal structure, the composition dependence of the hydrogen content, and the hydrogen absorption and desorption properties of the recovered hydrides were investigated. The Mn_xAl_{1-x} hydrides (x = 0.9, 0.8, and 0.7) with a hexagonal close-packed structure were formed at 9 GPa and 750°C, and were recovered at ambient conditions. The thermodynamic stability and hydrogen composition of the hydrides were found to decrease monotonically with increasing aluminum concentration. The former trend is likely attributable to the fact that elemental aluminum exhibits only negligible hydrogen solubility even under high pressure. The

decrease in hydrogen concentration with increasing Al content, is attributed to the preferential occupation, by hydrogen atoms, of octahedral sites coordinated by six Mn atoms or by five Mn atoms and one Al atom in Mn–Al alloys.

1. Introduction

Hydrogen storage alloys have attracted interest for a number of years for their high volumetric hydrogen capacities [1]. They store atomic hydrogen in the solid state, resulting in volumetric hydrogen densities exceeding gaseous densities at ambient pressure 1,000-fold. They absorb and desorb hydrogen reversibly under a hydrogenation pressure of around 1 MPa around room temperature (27°C). However, achieving high gravimetric hydrogen densities while reducing material costs remains a key challenge.

The conventional materials were synthesized using the design guideline for hydrogen storage alloys, consisting of metals with high and low affinities for hydrogen. Metals in groups I–V have a high affinity with hydrogen, whereas those in groups VI–XIII (except for Pd) have a low affinity with hydrogen. However, this guideline limits the choice of elements. Since lightweight and inexpensive metals have already been extensively explored, the discovery of novel lightweight and low-cost alloy hydrides is all the more challenging. To address this challenge of discovering novel hydrides, we attempted to

hydrogenate alloys consisting only of metals with a low affinity for hydrogen, especially cost-effective and lightweight aluminum (Al) and transition metals (*TM*). We used a high-pressure and high-temperature technique to search for novel alloy hydrides because hydrogen has a high chemical potential and a high solubility in a metal under hydrogenation pressures above 1 GPa [2].

We previously reported the formation of the Al-based hydrides Al_2CuH_x [3] and Al_3FeH_4 [4] under high pressure and high temperature. Notably, the gravimetric hydrogen density of Al_3FeH_4 is approximately 3 wt.%, approximately twice that of $LaNi_5H_6$. We thus found that Al-based alloys can be hydrogenated. We therefore aimed to clarify whether *TM*-based *TM*–Al alloys can also be hydrogenated. In this study, we attempted to synthesize manganese (Mn)-based Mn–Al alloy hydrides under high pressure and high temperature.

This study focused on Mn-based alloys because Mn is cost-effective metal. Mn-based alloys with C14-type Laves phase structure, $TiMn_{1.5}$ and $ZrMn_2$ can be hydrogenated to form the hydrides with the gravimetric hydrogen densities of 1.8 wt% and 1.7wt%, respectively [5][6]. To improve the hydrogen absorption properties, a number of studies have been conducted on hydrogenating $TiMn_2$-basd alloys and $ZrMn_2$-basd alloys, where Mn was substituted by some transition metals [7-11]. However, it has not been reported

that Mn-based alloys consisting only of metals with a low affinity for hydrogen.

Manganese can be hydrogenated above 0.6 GPa and 175°C to form the hydride with the atomic ratio between hydrogen and metal atoms (H/M) ~ 1.0, and the gravimetric hydrogen density, approximately 1.0 wt% at 2.8 GPa and 350°C [12]. Antonov *et al*. reported the pressure–temperature (*p*–*T*) phase diagram of the Mn–H system by measuring X-ray powder diffraction of recovered Mn–H that was quenched at −180°C after hydrogenation under high pressure and high temperature [13]. Fukai *et al*. obtained the *p*–*T* phase diagram of the Mn–H system by using the in-situ synchrotron radiation x-ray powder diffraction technique [14]. Fukai *et al*. reported that Mn–H forms a face-centered cubic (fcc) phase at 3–6 GPa and above 700°C, a hexagonal close-packed (hcp) phase at 3–7 GPa and 500°C–700°C, and a double hexagonal close-packed (dhcp) phase at 4–7 GPa and 700°C–800°C. The crystal structures of Mn–H depend on the hydrogen pressure and temperature.

In the present study, we attempted to synthesize Mn-based Mn–Al hydrides under high pressure and high temperature to clarify whether *TM*-based *TM*–Al alloys can also be hydrogenated. Mn-based Mn_xAl_{1-x} alloys (x = 0.9, 0.8, and 0.7) were hydrogenated at 9 GPa and 750°C to form Mn–Al hydrides. We investigated the crystal structure, the composition dependence of the hydrogen content, and the hydrogen absorption and

desorption properties of the recovered hydrides.

2. Methods

Mn–Al alloys produced by solid-state reactions under high pressure were used as the starting materials. Mn–Al alloys are generally difficult to produce by using an arc furnace because the vapor pressure of Mn is much higher than that of Al. In contrast, solid-state reactions under high pressure take place in a closed space, enabling the synthesis of alloys with target compositions even when the vapor pressures of the constituent elements differ strongly. Mn (Soekawa Chemicals Corporation, Japan, purity 99.95 %) and Al (NewMet Corporation, Japan, purity 99.95 %) powders were mixed with nominal atomic ratios 1:9, 1:4, and 3:7 using an agate mortar and pestle. The mixed powders were compacted into disks with 5.0 mm diameter and 4.0 mm thickness. The disks were placed into a high-pressure cell (Figure 1 (a)) and pressurized to 0.5 GPa at room temperature (25°C) and subsequently heated to 1100°C at a heating rate of 50°C/min. The samples were held at 0.5 GPa and 1100°C for 1 min and subsequently quenched at room temperature. Thereafter, the samples were decompressed to ambient pressure and recovered at ambient conditions. A 1500-ton cubic-type multi-anvil apparatus was used to generate high-pressure and high-temperature conditions.

The Mn–Al alloy disks were ground using an agate mortar and pestle, and then the powders were compacted into disks with 1.0 mm diameter and 0.5 mm thickness. The Mn–Al alloy disks, and also disks of Mn (Soekawa Chemicals Corporation, Japan, purity 99.95 %) used for comparison, were placed in cells (Figure 1 (b)) designed for high-pressure hydrogenation experiments [15]. The samples were pressurized to 9 GPa at room temperature and subsequently heated to 750°C at a heating rate of 100°C/min. They were immersed in fluid hydrogen at 9 GPa and 750°C for 2 hours before being cooled to room temperature at a cooling rate of 100°C/min. Thereafter, the samples were decompressed to ambient pressure and recovered at ambient conditions. The method originally developed by Fukai [16] was used to perform high-pressure and high-temperature hydrogenation experiments using a 180-ton cubic-type multi-anvil apparatus. AlH_3 powder was used as the internal hydrogen source.

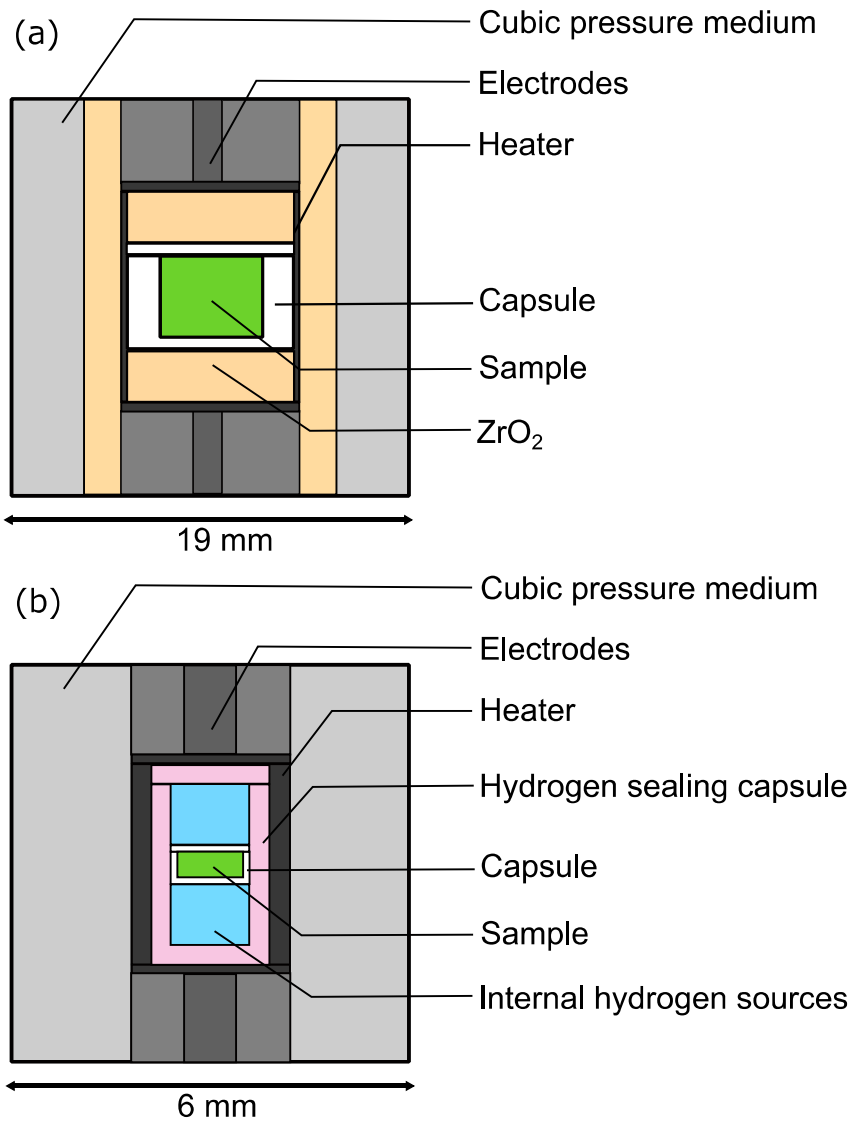


Figure 1 Schematic cross-sectional diagrams of the high-pressure cell design. (a) High-pressure cell assembly used to prepare the starting materials. (b) High-pressure cell assembly used for performing high-pressure hydrogenation reactions.

The hydrogenation reactions of Mn_xAl_{1-x} alloys (x = 0.9, 0.8, and 0.7) and pure Mn were investigated using in situ synchrotron radiation x-ray powder diffraction measurements. The measurements were performed using a 180-ton cubic-type multi-anvil

apparatus installed onto the BL14B1 beamline of SPring-8, Japan. White x-rays from a bending magnet source were used as incident x-rays, irradiating samples in a cubic pressure medium after passing through a narrow anvil gap. X-rays diffracting from the samples passed through another anvil gap on the site opposite to the incident side and were collected using the energy-dispersive method with a Germanium solid-state detector. The incident beam was 50 μm high and 200 μm wide. The diffraction angle was set to 2θ = 6°, and a profile was obtained over a 120 s period.

The obtained hydrides were recovered at ambient conditions. The evolution of hydrogen from the recovered samples was investigated using a thermal desorption spectroscopy system for hydrogen analysis (HTDS; R-DEC Co. Ltd., Japan, HTDS-003). The recovered samples were heated to 300°C under vacuum at a heating rate of 1.7°C/min while using HTDS to determine the amount and temperature of hydrogen released from the recovered samples. A conventional powder x-ray diffractometer (Rigaku, Japan, R-axis rapid) was used to examine the crystal structures of the starting materials and the recovered samples at ambient conditions. Notably, hydrogen-release temperatures under vacuum, as determined using HTDS, are frequently affected by the hydrogen desorption kinetics and do not reflect thermodynamic stability

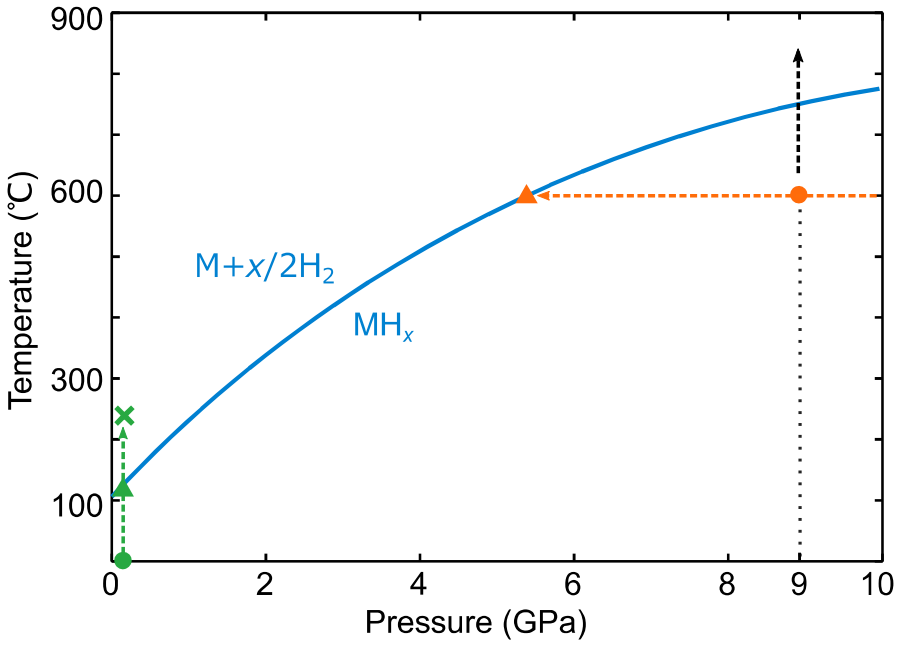


Figure 2 Schematic of the experimental *p*–*T* paths done in the present study. The blue curve shows the equilibrium *p*–*T* conditions for the hydrogenation reaction of Metal (M). The green and orange doted lines represent *p*–*T* paths for thermal desorption spectroscopy (HTDS) and in situ high-pressure experiments, respectively. In HTDS measurements, the equilibrium temperature is relatively low (green triangle), and exceeded by the experimentally observed decomposition temperature (green cross) for kinetic reasons. In contrast, the *p*–*T* conditions achieved in high-pressure measurements (orange triangle) are less influenced by kinetic limitations. Heating a sample under a high pressure (dotted black line) makes the dhcp phase appear before decomposition.

Near ambient pressure, the equilibrium temperature is low, as indicated by the green closed triangle in Figure 2. The method for determining the equilibrium curve plotted in Figure 2 is described in the Supplementary Material. The main source of the effect of kinetics on the hydrogen desorption temperatures measured by HTDS is likely to be the

surface oxide layers, which allow the hydrides to be dehydrogenated above the equilibrium temperature (Figure 2, green cross). Dehydrogenation at high temperatures, under conditions that suppress these kinetic effects, enables the evaluation of the thermodynamic stability of the hydrides.

Several *p*–*T* paths for decomposing hydrides at high temperatures are possible. The simplest *p*–*T* path, from an experimental perspective, involves heating a hydride at a high pressure (Figure 2, black dotted line). However, this approach does not apply to Mn_xAl_{1-x} hydrides (x = 0.9, 0.8, and 0.7) and MnH, which have an hcp structure. Both the Mn_xAl_{1-x} hydrides and MnH with hcp structures formed at 9 GPa and 750°C were transformed into dhcp upon heating. Consequently, simple heating experiments were not adopted in the present study.

We employed an alternative *p*–*T* path to performing heating experiments at high pressure. After forming the hcp Mn_xAl_{1-x} hydrides (x = 0.9, 0.8, and 0.7) and MnH at 9 GPa and 750°C, the hydrides were cooled to 600°C at 9 GPa and subsequently decompressed toward ambient pressure while remaining 600°C (Figure 2, orange dotted line). The dehydrogenation reactions of the hcp Mn_xAl_{1-x} hydrides and MnH were detected using the in-situ synchrotron radiation x-ray powder diffraction measurements. The thermodynamic stability of each hydride was evaluated from its decomposition

pressure at 600°C. A low decomposition pressure corresponds to a high thermodynamic stability.

Each sample following the above *p*–*T* path was first pressurized to 9 GPa at room temperature and then heated to 750°C at a rate of 100°C/min. The sample was then cooled to 600°C and then decompressed at 600°C. The pressure at the sample position during the decompression was determined from the unit cell volume of NaCl measured by x-ray diffraction (XRD), based on its equation of state [17]. The pressure calibration—relating the applied press load to the actual sample pressure—was performed separately. The decomposition pressures of the hydrides were then determined using this calibration.

3. Results

3.1 Crystal structures of the starting materials

The crystal structures of the starting materials were determined using a conventional powder x-ray diffractometer. Figure 3 shows XRD patterns of the Mn_xAl_{1-x} alloys (x = 0.9, 0.8, and 0.7) as the starting materials. The diffraction peaks in all samples were indexed by cubic unit cells. The lattice volumes per formula unit of Mn and Mn_xAl_{1-x} alloys are summarized in Table 1. Mn_xAl_{1-x} alloys form the β-Mn-type solid-solution phases with cubic unit cells, which are the most thermodynamically stable phases [18]. The XRD patterns correspond to the reported results. Because Al has a larger atomic

radius than Mn, the lattice volumes increase with the Al content, indicating the formation of β-Mn-type Mn–Al solid-solution phases.

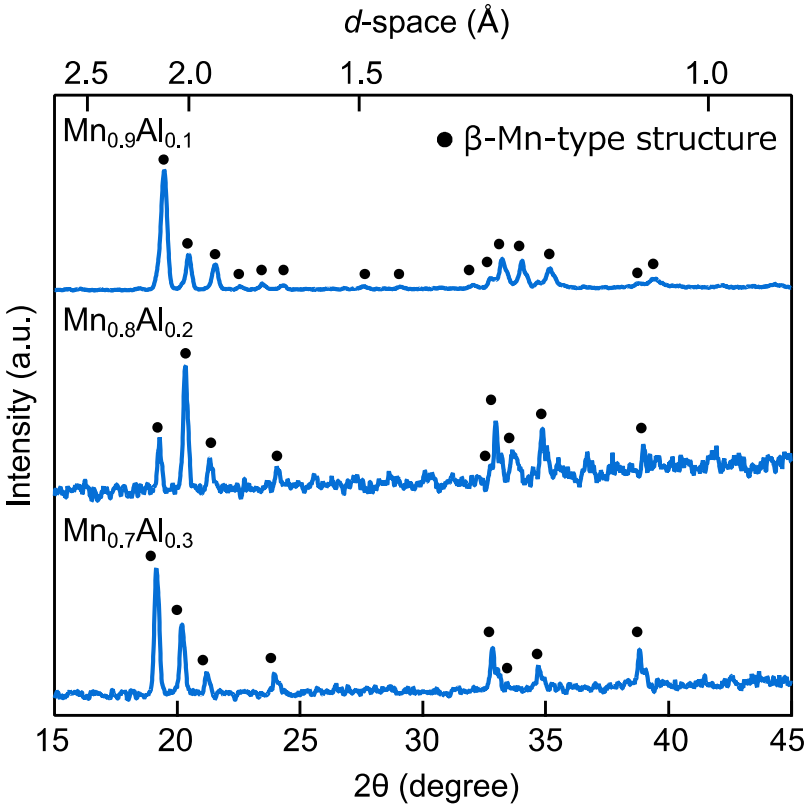


Figure 3 X-ray diffraction patterns of Mn_xAl_{1-x} alloys (x = 0.9, 0.8, and 0.7) as starting materials. The circles represent diffraction peaks from a β-Mn-type structure phase, respectively.

Table 1 Nominal composition, the crystal structure type, and lattice volume per formula unit of Mn and Mn_xAl_{1-x} alloys (x = 0.9, 0.8, and 0.7). Numbers in parentheses represent errors.

Nominal composition	Crystal structure type	Lattice volume per formula unit (Å^3/ f.u.)
Mn	α-Mn-type	12.1(1)
$Mn_{0.9}Al_{0.1}$	β -Mn-type	12.5(2)
$Mn_{0.8}Al_{0.2}$	β -Mn-type	12.8(2)
$Mn_{0.7}Al_{0.3}$	β -Mn-type	13.0(1)

3.2 In situ synchrotron radiation x-ray diffraction measurements of the hydrogenation reactions of Mn_xAl_{1-x} alloys (x = 0.9, 0.8, and 0.7).

The β-Mn-type Mn_xAl_{1-x} alloys (x = 0.9, 0.8, and 0.7) were immersed in fluid hydrogen at 9 GPa and 750°C to allow the formation of hcp Mn_xAl_{1-x} hydrides. In-situ synchrotron radiation x-ray powder diffraction profiles of the β-Mn-type $Mn_{0.7}Al_{0.3}$ alloy in fluid hydrogen at 9 GPa are plotted in Figure 4. The alloy maintained its crystal structure even, after being pressurized to 9 GPa at room temperature. The crystal structure began to transform from the β-Mn-type structure to an hcp structure above 640°C. Upon heating to 750°C, the alloy became completely converted into a single hcp phase. The hcp phase remained stable at 9 GPa and 750°C for 2 hours and the sample was subsequently cooled

to room temperature and decompressed to ambient pressure. The hcp phase retained its crystal structure during cooling and decompression and recovered at ambient conditions.

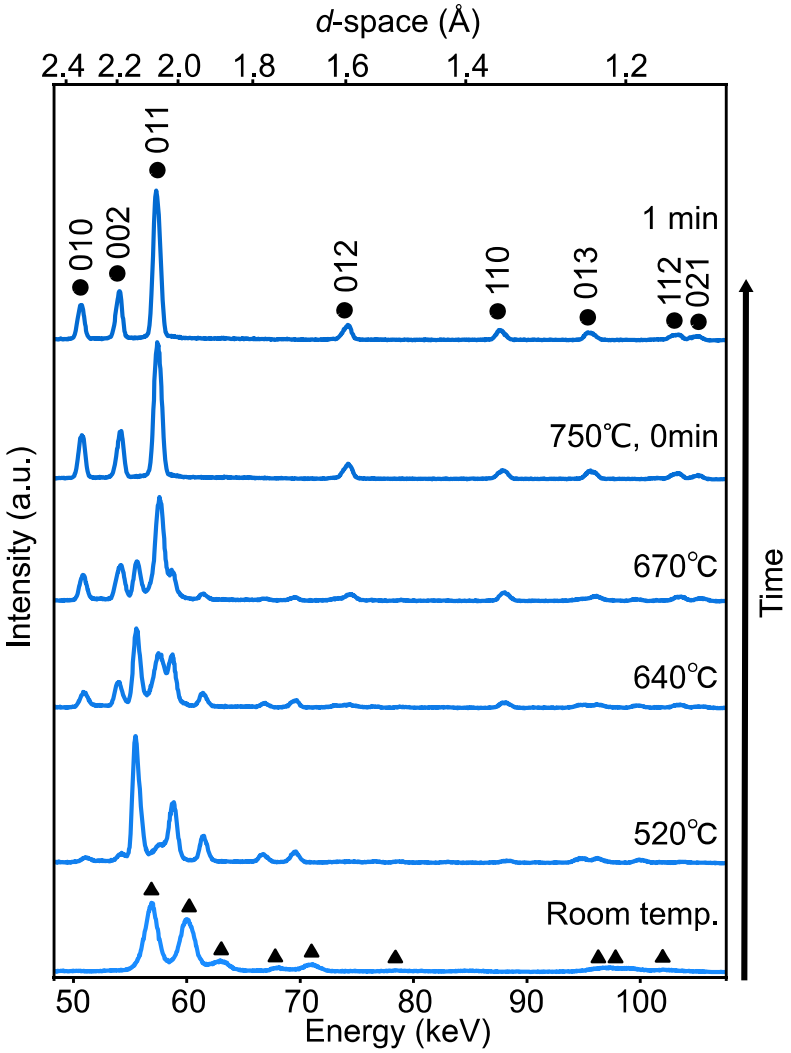


Figure 4 In situ synchrotron-radiation x-ray powder diffraction profiles of $Mn_{0.7}Al_{0.3}$ alloy in fluid hydrogen at 9 GPa. The triangles and circles represent diffraction peaks from a β-Mn-type structure phase and from an hcp structure phase, respectively.

The β-Mn-type Mn_xAl_{1-x} alloys (x = 0.9 and 0.8) and α-Mn-type Mn transformed into an

hcp structure while placed in fluid hydrogen at 9 GPa and 750°C for 2 hours. All the formed hcp phases were recovered at ambient conditions. The lattice parameters of the recovered samples at ambient conditions are summarized in Table 2. When the $Mn_{0.7}Al_{0.3}$ alloy was pressurized and heated under the same *p*–*T* conditions in the absence of hydrogen, the hcp phase was not recovered at ambient conditions. In this case, the crystal structure of the starting material remained unchanged by the high-pressure and the high-temperature treatment. The hcp phases were confirmed to be formed by hydrogenation reactions.

Table 2 Lattice parameters of the hydrogenated samples

The hydrogenated sample	*a* (Å)	*c* (Å)	*V* (Å^3)	*c*/*a*
Mn	2.690(1)	4.364(2)	27.34(2)	1.62
$Mn_{0.9}Al_{0.1}$	2.690(1)	4.362(2)	27.34(2)	1.62
$Mn_{0.8}Al_{0.2}$	2.685(1)	4.345(2)	27.13(2)	1.62
$Mn_{0.7}Al_{0.3}$	2.695(1)	4.357(2)	27.40(2)	1.62

3.3 *Hydrogen evolution from the recovered hcp phases*

The hydrogen release temperatures and the hydrogen content of the recovered hcp phases were determined using HTDS. Figure 5 summarizes the hydrogen desorption profiles of the recovered hcp phases when heated to 300°C under vacuum. Hydrogen was released

from all the recovered samples, confirming the recovery of hydrides at ambient conditions. $Mn_{0.9}Al_{0.1}$ hydride begin to release hydrogen at approximately 50°C, approximately 20°C lower than pure MnH, whereas Mn_xAl_{1-x} hydrides (x = 0.8 and 0.7) begin to release hydrogen at nearly the same temperatures as MnH.

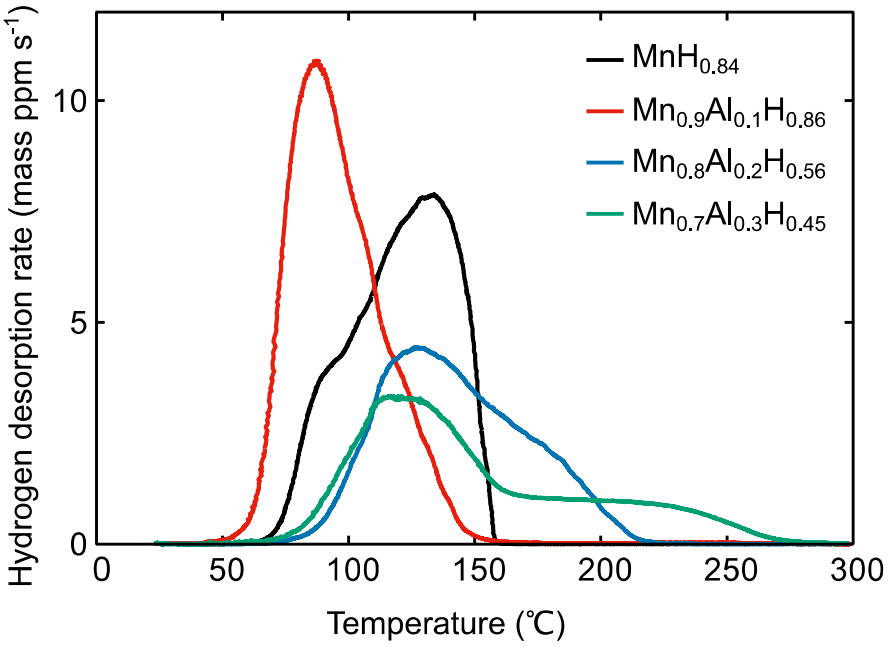


Figure 5 Hydrogen desorption profiles of the recovered Mn_xAl_{1-x} hydrides (x = 0.9, 0.8, and 0.7) and MnH. Red, blue, green, and black lines represent the data of $Mn_{0.9}Al_{0.1}H_{0.86}$, $Mn_{0.8}Al_{0.2}H_{0.56}$, $Mn_{0.7}Al_{0.3}H_{0.45}$, and $MnH_{0.84}$, respectively.

The gravimetric hydrogen densities and H/M values of the recovered hydrides are summarized in Table 3. The gravimetric hydrogen densities decrease with increasing Al content. The composition dependence of H/M values is discussed in Section 4.3.

Table 3 Gravimetric hydrogen densities and H/M values of the recovered hydrides

The hydrogenated sample	Gravimetric hydrogen density (wt.%)	H/M
Mn	1.52	0.84
$Mn_{0.9}Al_{0.1}$	1.63	0.86
$Mn_{0.8}Al_{0.2}$	1.13	0.56
$Mn_{0.7}Al_{0.3}$	0.97	0.45

3.4 Thermodynamic stabilities of Mn_xAl_{1-x} hydrides (x = 0.9, 0.8, and 0.7)

Although the hydrogen-release temperatures of the recovered hydrides were determined using HTDS (Section 3.3), the results may not accurately reflect the intrinsic thermodynamic stabilities of the hydrides, owing to the influence of the surface oxide layers, which suppresses the hydrogen desorption reaction [19]. To evaluate the hydride thermodynamic stabilities, the dehydrogenation *p*–*T* conditions at high pressure and high temperature were measured. The results were largely unaffected by the surface oxide layer. Figure 6 (a) shows the in-situ synchrotron radiation x-ray powder diffraction profiles obtained during the dehydrogenation reaction of the hcp $Mn_{0.7}Al_{0.3}$ hydride upon decompression at 600°C.

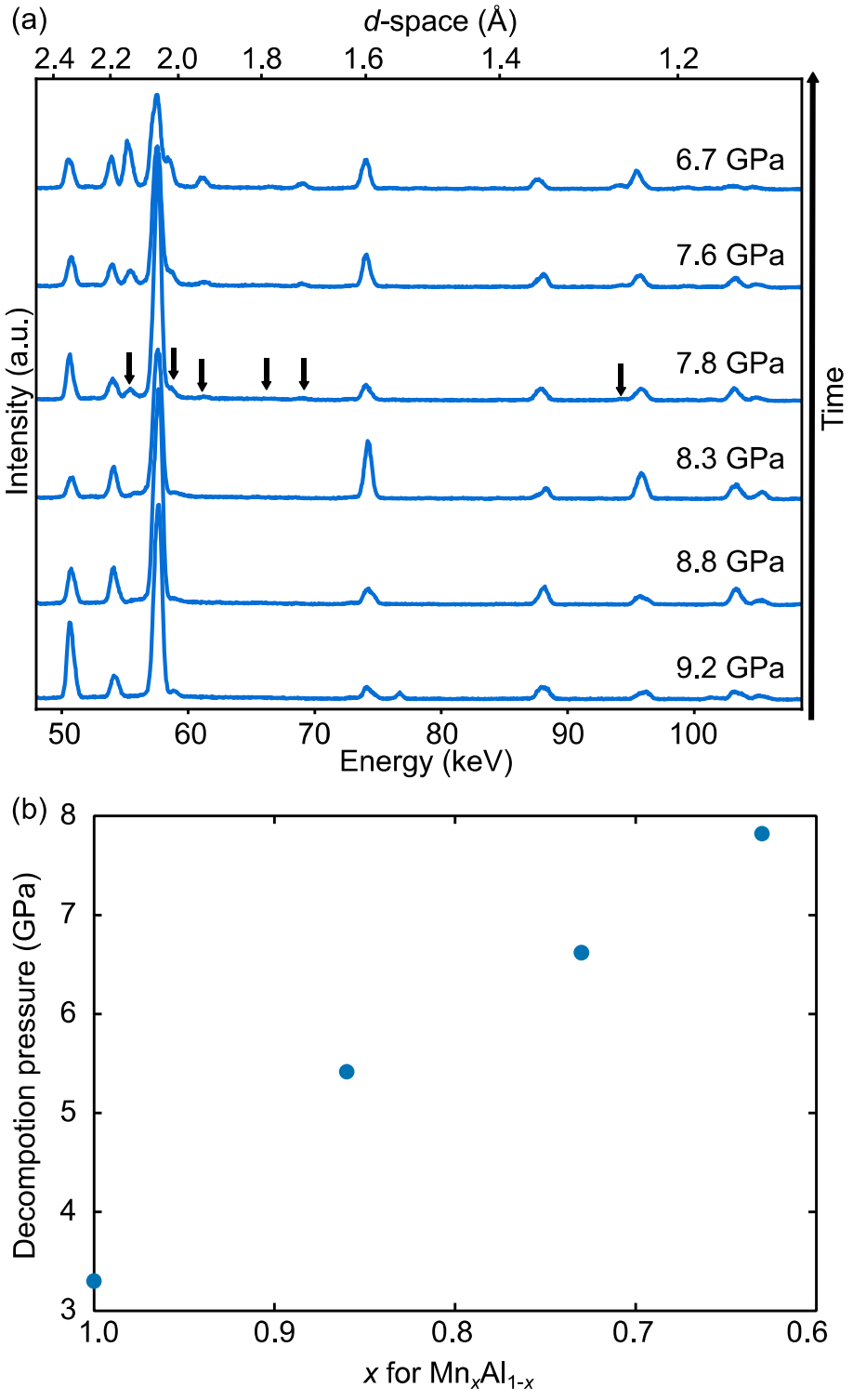


Figure 6 (a) In-situ synchrotron radiation x-ray powder diffraction profiles obtained during the dehydrogenation reaction of the hcp $Mn_{0.7}Al_{0.3}$ hydride upon decompression at 600°C. The arrows indicate diffraction peaks from the β-Mn-type Mn–Al alloy. (b) Relationship between the decomposition pressure and the composition.

After the formation of the hcp $Mn_{0.7}Al_{0.3}$ hydride at 9 GPa and 750°C in fluid hydrogen, the sample was cooled to 600°C and decompressed toward ambient pressure at 600°C. Diffraction peaks from the β-Mn-type Mn–Al alloy appeared at 7.5 GPa and 600°C. The peak intensities increased slowly with decreasing pressure. However, the sample could not be decompressed to ambient pressure at 600°C because of a limitation of the high-pressure apparatus. Therefore, the sample was cooled to room temperature at 6.7 GPa although the dehydrogenation reaction was not yet complete. The same experiments were performed for Mn and the Mn_xAl_{1-x} alloys (x = 0.9 and 0.8). The hcp Mn_xAl_{1-x} hydrides (x = 0.9 and 0.8) decomposed to the β-Mn-type Mn–Al alloys during decompression at 600°C in the same manner as the $Mn_{0.7}Al_{0.3}$ hydride, whereas the hcp MnH decomposed to form α-Mn. The decomposition pressures upon decompression at 600°C are summarized in Figure 6 (b). The decomposition pressure monotonously increases with Al content, indicating a decrease in the hydride thermodynamic stability. The dependence of thermodynamic stability on Al composition is discussed in Section 4.3.

4. Discussion

4.1 Single hcp phases of Mn_xAl_{1-x} hydrides (x = 0.9, 0.8, and 0.7)

Hydrogen release upon heating under vacuum (Section 3.3) confirms that the recovered single hcp phases were hydrides. However, it has been reported that Mn hydrogenation

yields hcp MnH under the same hydrogenation conditions as the hcp Mn_xAl_{1-x} hydrides (x = 0.9, 0.8, and 0.7) [14]. A comparison of the p–T phase diagram of Mn–H (Figure 7) with the hydrogenation conditions of the Mn_xAl_{1-x} hydrides indicates that these conditions fall within the stability field of hcp MnH (blue circle in Figure 7). It cannot be ruled out that the recovered hcp single phase corresponds not to Mn_xAl_{1-x} hydrides but to a hydride of pure Mn. However, the hydrogen-release temperatures and the hydrogen content of the recovered samples differed from those of MnH (Figure 5). Therefore, recovered single hcp phases correspond to Mn_xAl_{1-x} hydrides, in which some of the Mn atoms in hcp MnH are substituted by Al atoms.

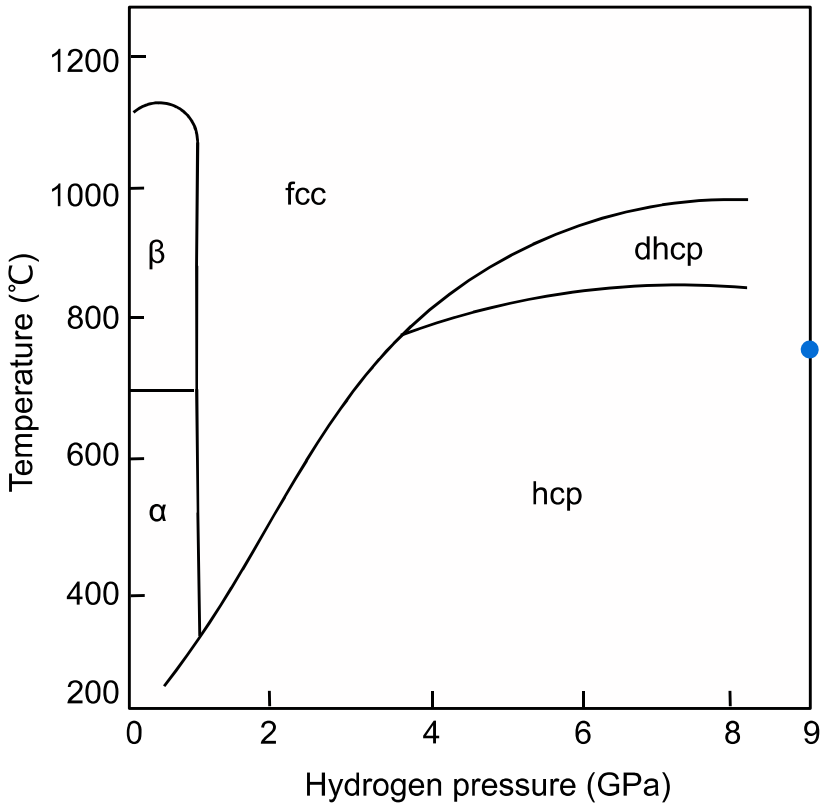


Figure 7 *p–T* phase diagram of the Mn–H system.
The figure was redrawn from reference [14]. The blue circle represents the hydrogenation conditions of the Mn_xAl_{1-x} hydrides (x = 0.9, 0.8, and 0.7).

4.2 Composition dependence of the hydrogen release temperatures

The hydrogen desorption profiles show that the hydrogen-release temperatures of MnH and Mn_xAl_{1-x} hydrides (x = 0.9, 0.8, and 0.7) under vacuum depend on the alloy composition. Although MnH is metastable at ambient conditions, it does not desorb hydrogen even over a 1 month period. Hydrogen desorption behaviors under vacuum indicate that the hydrides are kinetically stable. By contrast, the decomposition pressures of the hydrides at 600°C (Section 3.4) are expected to reflect their thermodynamic

stabilities, which decrease monotonously with increasing Al content.

$Mn_{0.9}Al_{0.1}$ hydride releases hydrogen at a lower temperature than MnH as shown in Figure 5, consistent with their relative thermodynamic stabilities. In contrast, the hydrogen desorption profile peaks of Mn_xAl_{1-x} hydrides (x = 0.8 and 0.7) appear at higher temperatures than those of MnH. This composition dependence of the hydrogen-release temperatures is attributed to the presence of a surface oxide layer. It is generally known that a hydride's surface oxide layer suppresses the hydrogen desorption reaction [19]. Consequently, Al-based hydrides tend to release hydrogen at a temperature higher than their hydrogen-release equilibrium temperature.

4.3 Al composition dependence of hydrogen composition

The hydrogen concentrations in MnH and Mn_xAl_{1-x} hydrides (x = 0.9, 0.8, and 0.7) with an hcp structure were evaluated using HTDS as described in Section 3.3. The H/M values decreased with increasing Al content (Table 3). We hypothesized that this observed compositional dependence can be attributed to the atomic species forming the hydrogen occupancy sites in the hcp hydrides.

The hydrogen occupancy sites in the Mn_xAl_{1-x} hydrides can be inferred from those in MnH because MnH and the alloy hydrides are isostructural. In MnH, hydrogen atoms occupy the octahedral (O) sites, which are coordinated by six Mn atoms [20]. The

Mn_xAl_{1-x} hydrides can display seven types of O-sites, with local coordination environments described as Mn_6 (O-sites coordinated by six Mn atoms), Mn_5Al_1 (O-sites coordinated by five Mn atoms and one Al atom), Mn_4Al_2 (O-sites coordinated by four Mn atoms and two Al atoms), Mn_3Al_3 (O-sites coordinated by three Mn atoms and three Al atoms), Mn_2Al_4 (O-sites coordinated by two Mn atoms and four Al atoms), Mn_1Al_5 (O-sites coordinated by one Mn atom and five Al atoms), and Al_6 (O-sites coordinated by six Al atoms). Because the solubility of hydrogen in Al is less than 10^{-2} even under a high hydrogen pressure of 10 GPa [2], the stability of hydrogen at these sites is expected to decrease as the ratio of Al to Mn atoms at these sites increases.

We subsequently calculated the occurrence probability for each O-site type present in the alloys. The occurrence probability of an O-site in Mn_xAl_{1-x} alloy described by Mn_yAl_{6-y} can be described as follows:

$$p = \binom{6}{y} x^y (1-x)^{6-y} \quad (1)$$

where $\binom{6}{y}$ denotes the binomial coefficient, i.e., the number of possible combinations of y Mn atoms arranged on six metal sites. The calculated p values for each O-site type present in the alloys are summarized in Supplementary Material S2.

The H/M values of the Mn_xAl_{1-x} hydrides were calculated using the occurrence probabilities of the O-sites, as described below. Because full O-site occupancy in MnH

and in the Mn_xAl_{1-x} hydrides corresponds to H/M = 1, the H/M values of these metal hydrides are equal to the summed probabilities for the O-sites that hydrogen can occupy. As discussed above, Al-based O-sites are expected to destabilize interstitial hydrogen; we therefore assumed that hydrogen preferentially occupies the Mn-based O-sites. When only Mn_6 O-sites (model A) are occupied by hydrogen atoms and the other O-sites remain vacant, the Mn-composition dependence of the H/M value is represented by the light green curve in Figure 8. When both Mn_6 O-sites and Mn_5Al_1 O-sites (model B) are occupied and the other O-sites are vacant, the Mn-composition dependence of the H/M value is represented by the darker green curve in Figure 8. Results for other occupancy models are also shown in Figure 8.

Figure 8 also shows the experimentally determined H/M values for the recovered MnH and Mn_xAl_{1-x} hydrides (Figure 8, red squares). The experimentally determined hydrogen concentration agrees well with the calculated values for model B, indicating that hydrogen atoms in the Mn_xAl_{1-x} hydrides can occupy Mn_6 O-sites and Mn_5Al_1 O-sites.

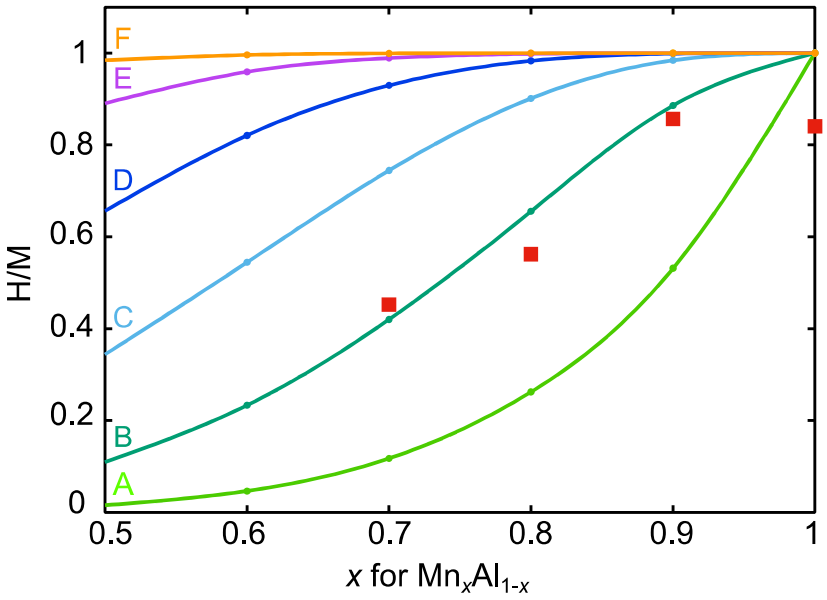


Figure 8 Composition dependence of H/M for the recovered MnH and Mn_xAl_{1-x} alloy hydrides (red squares). The dependence of the hydrogen content on the Mn composition is represented by the light green, dark green, light blue, dark blue, purple, and orange curves representing the following models: all Mn_6 O-sites (model A), Mn_6 and Mn_5Al_1 O-sites (model B), Mn_6, Mn_5Al_1, and Mn_4Al_2 O-sites (model C), Mn_6, Mn_5Al_1, Mn_4Al_2, and Mn_3Al_3 O-sites (model D), Mn_6, Mn_5Al_1, Mn_4Al_2, Mn_3Al_3, and Mn_2Al_4 O-sites (model E), and Mn_6, Mn_5Al_1, Mn_4Al_2, Mn_3Al_3, Mn_2Al_4, and Mn_1Al_5 O-sites (model F).

5. Conclusions

Mn-based Mn_xAl_{1-x} alloys (x = 0.9, 0.8, and 0.7) were hydrogenated at 9 GPa and 750°C to form hcp alloy hydrides. The thermodynamic stability decreased with increasing Al content. In contrast, the hydrogen-release temperatures of the Mn_xAl_{1-x} alloys (x = 0.8 and 0.7) were higher than those of MnH because the surface oxide layer on the hydride suppresses the hydrogen desorption reaction. Hydrogen atoms in Mn_xAl_{1-x} hydrides preferentially occupy Mn_6 O-sites and Mn_5Al_1 O-sites. Consequently, the hydrogen

concentration decreased with increasing Al content because of the reduction of these O-site occupancies. These results provide a guideline for designing Al–*TM* alloy hydrides. Specifically, hydrides with a high hydrogen content are expected to be obtained in the Al-rich composition region, as reported in the Al–Fe system because, in Mn-rich hydrides, increasing the amount of Al tends to destabilize the hydrides and reduce the hydrogen content. On the contrary, hydrides with lower hydrogen-release temperatures may be designed in the Mn-rich composition region.

CRediT authorship contribution statement

Reina Utsumi: Conceptualization, Validation, Formal analysis, Investigation, Resources, Data curation, Writing – original draft, Visualization, Funding acquisition. **Saya Ajito**: Investigation, Resources, Formal analysis, Writing – review & editing. **Shigeyuki Takagi**: Investigation, Resources, Formal analysis, Visualization, Writing – review & editing. **Yuki Nakahira**: Investigation, Resources, Formal analysis, Writing – review & editing. **Hiroyuki Saitoh**: Conceptualization, Validation, Investigation, Visualization, Writing – review & editing, Supervision, Project administration, Funding acquisition. **Tetsu Watanuki**: Writing – review & editing, Supervision, Project administration. **Toyoto Sato**: Investigation, Resources, Writing – review & editing. **Eiji Akiyama**: Investigation, Resources, Writing – review & editing. **Shin-ichi Orimo**: Writing – review

& editing, Supervision, Project administration, Funding acquisition.

Declaration of Competing Interest

The authors have filed a patent related to the materials reported in this work (JP-2023-134157).

Acknowledgments

We are grateful to Yukari Shinomoto for providing technical support. This work was supported by JSPS KAKENHI Grant-in-Aid for JSPS Fellows Grant Number 23KJ1856, Grant-in-Aid for Early-Career Scientists Grant Number 26K17667, and GteX program Japan Grant Number JPMJGX23H1. The synchrotron radiation X-ray diffraction experiments were performed using a QST experimental station at the QST beamline BL14B1 and SPring-8, with the approval of the Japan Synchrotron Radiation Research Institute JASRI (Proposal Nos. 2023A3651, 2023A3652, 2023B3652, 2024A3652, 2024B3652, 2025A3651, 2025B3651, 2025B3652). In situ X-ray diffraction profiles were analyzed using a program, PDIndexer developed by Dr. Yusuke Seto.

References

[1] G. G. Libowitz, H. F. Hayes, and T. R. P. J. Gibb, The System Zirconium–Nickel and Hydrogen, J. Phys. Chem., 62 (1958) 76–79,

https://doi.org/10.1021/j150559a019.

[2] H. Sugimoto and Y. Fukai, Solubility of hydrogen in metals under high hydrogen pressures: Thermodynamical calculations, Acta Metall. Mater., 40 (1992) 2327–2336, https://doi.org/10.1016/0956-7151(92)90151-4.

[3] H. Saitoh, S. Takagi, N. Endo, A. Machida, K. Aoki, S. Orimo, and Y. Katayama, Synthesis and formation process of Al_2CuH_x: A new class of interstitial aluminum-based alloy hydride, APL Materials, 1 (2013) 032113, https://doi.org/10.1063/1.4821632.

[4] H. Saitoh, T. Sato, M. Tanikami, K. Ikeda, A. Machida, T. Watanuki, T. Taguchi, S. Yamamoto, T. Yamaki, S. Takagi, T. Otomo, and S. Orimo, Hydrogen storage by earth-abundant metals, synthesis and characterization of $Al_3FeH_{3.9}$, Materials and Design, 208 (2021) 109953, https://doi.org/10.1016/j.matdes.2021.109953.

[5] T. Gamo, Y. Moriwaki, N. Yanagihara, T. Yamashita, and T. Iwaki, Formation and properties of titanium-manganese alloy hydrides, INT. J. HYDROG. ENERGY, 10 (1985) 39–47, https://doi.org/10.1016/0360-3199(85)90134-X.

[6] H. Fujii, M. Saga, and T. Okamoto, Magnetic, crystallographic and hydrogen absorption properties of YMn_2 and $ZrMn_2$ hydrides, J. Less Com. Met., 130 (1987) 25–31, https://doi.org/10.1016/0022-5088(87)90083-X.

[7] D. Shaltiel, I. Jacob, and D. Davidov, Hydrogen absorption and desorption properties of AB_2 laves-phase pseudobinary compounds, J. Less Com. Met., 53 (1977) 117–131, https://doi.org/10.1016/0022-5088(77)90162-X.

[8] V. K. Sinha and W. E. Wallace, Hydrides of $ZrMn_2$-based alloys substoichiometric in zirconium for engineering applications, J. Less COm. Met., 106 (1985) 199–210, https://doi.org/10.1016/0022-5088(85)90255-3.

[9] M. Y. Song, I. H. Kwon, D. S. Ahn, and M. S. Sohn, Improvement in the electrochemical properties of $ZrMn_2$ hydrides by substitution of elements, Metals Mater Int., 7 (2001) 257–263, https://doi.org/10.1007/BF03026984.

[10] Y. Zhang, C. Li, W. Zhang, X. Wei, J. Li, Y. Qi, and D. Zhao, Research and application of Ti–Mn-based hydrogen storage alloys, J. Iron and Steel Res. Int., 30 (2023) 611–625, 2023, https://doi.org/10.1007/s42243-022-00905-1.

[11] J. Liu, L. Sun, J. Yang, D. Guo, D. Chen, and L. Yang, Ti – Mn hydrogen storage alloys : from properties to applications, RSC Adv., 12 (2022) 35744–35755, https://doi.org/10.1039/d2ra07301c.

[12] A. San-Martin and F.D. Manchester, H-Mn (Hydrogen-Manganese), Phase Diagrams of Binary Hydrogen Alloys, 27 (1996) 95–104.

[13] M. B. and F. E. W. V.E Antonov, T.E. Antonova, N.A. Chirin, E.G. Ponyatovsky,

T-P PHASE DIAGRAM OF THE Mn-H SYSTEM AT PRESSURES TO 4.4 GPa AND TEMPERATURES TO 1000°C, Scripta Materialia, 34 (1996) 1331–1336, https://doi.org/10.1016/1359-6462(95)00656-7.

[14] K. M. Y. Fukai, T. Haraguchi, H. Shinomiya, Constitution of the Mn–H system at high hydrogen pressures, Scripta Materialia, 46 (2002) 679–684, https://doi.org/10.1016/S1359-6462(02)00052-0..

[15] H. Saitoh, A. Machida, and K. Aoki, Synchrotron X-ray diffraction techniques for in situ measurement of hydride formation under several gigapascals of hydrogen pressure, Chinese Science Bulletin, 59 (2014) 5290–5301, https://doi.org/10.1007/s11434-014-0543-8..

[16] Y. Fukai and N. Okuma, Evidence of copious vacancy formation in Ni and Pd under a high hydrogen pressure, Jpn. J. Appl., 32 (1993) L1256–L1259, https://doi.org/10.1143/JJAP.32.L1256.

[17] D. L. Decker, Equation of State of NaCl and Its Use as a Pressure Gauge in High-Pressure Research, J. Appl. Phys., 36 (1965) 157–161, https://doi.org/10.1063/1.1713864.

[18] Åke Jansson, A thermodynamic evaluation of the Al-Mn system, Metall. Trans. A, 23 (1992) 2953–2962, https://doi.org/10.1007/BF02646113.

[19] S. Kato, M. Bielmann, K. Ikeda, S. Orimo, A. Borgschulte, and A. Züttel, Surface changes on AlH_3 during the hydrogen desorption, Applied Physics Letters, 96 (2010), 2008–2011, https://doi.org/10.1063/1.3269598.

[20] V.P. Zhebelev, V.A. Somenkov, E.G. Ponyatovskii, S.Sh. Shil'stein, and I.T. Belash, Structure of Ni and Mn Deuterides Syn- thesized at High Pressures, Inorganic Mater., 14 (1978) 1264–1266.